Available online at www.sciencedirect.com
SCIENCE DIRECT®
International Journal of Heat and Mass Transfer 49 (2006) 4608–4623
International Journal of HEAT and MASS TRANSFER
www.elsevier.com/locate/ijhmt

A numerical study of natural convection around a square, horizontal, heated cylinder placed in an enclosure

Arnab Kumar De *, Amaresh Dalal

Department of Mechanical Engineering, Indian Institute of Technology Kanpur, Kanpur 208 016, India

Received 25 May 2005; received in revised form 16 December 2005
Available online 22 June 2006

Abstract

In this paper, natural convection around a tilted heated square cylinder kept in an enclosure has been studied in the range of $10^3 \leqslant Ra \leqslant 10^6$. Streamfunction-vorticity formulation of the Navier–Stokes equation is solved numerically using finite-difference method in non-orthogonal body-fitted coordinate system. Detailed flow and heat transfer features for two different thermal boundary conditions are reported. Effects of the enclosure geometry has been assessed using three different aspect ratio placing the square cylinder at different heights from the bottom. The concept of heatfunction has been employed to trace the path of heat transport. It is found that the uniform wall temperature heating is quantitatively different from the uniform wall heat flux heating. Flow pattern and thermal stratification are modified, if aspect ratio is varied. Overall heat transfer also changes for different aspect ratio.

Keywords: Natural convection; Enclosure; Square cylinder; Uniform wall temperature; Uniform heat flux; Heatlines

1. Introduction

The phenomenon of natural convection in enclosure has been a subject of research over the years. Numerous references [1–3] deal with enclosures with flat walls due to its relevance to large scale natural phenomena in the fields of astrophysics, geophysics, atmospheric sciences and a wide range of engineering applications such as cooling of electronic equipments, solidification processes, growing crystals and solar collectors. They admit complex interactions between the finite fluid content inside the enclosure with the enclosure walls.

A large number of literature is available which deal with the study of natural convection in enclosures [4–8] with either vertical or horizontal imposed heat flux or temperature difference. Hadjisophocleous et al. [9] solved the natural convection of a square cavity problem by non-orthogonal boundary fitted coordinate system. However, they compared their results with that of de Vahl Davis [1] and Markatos and Perikleous [2] which is a regular geometry problem.

Buoyancy driven flow and heat transfer between a cylinder and its surrounding medium has been a problem of considerable importance. This problem has a wide range of applications. Energy storage devices, crop dryers, crude oil storage tanks, heat exchangers, spent fuel storage of nuclear power plants are a few to name. Larson et al. [10] carried out experimental study of temperature field around a heated horizontal cylindrical body in an isothermal rectangular enclosure. Roychowdhury et al. [11] analyzed the natural convective flow and heat transfer features for a heated cylinder kept in a square enclosure with different thermal boundary conditions. Elepano and Oosthuizen [12] carried out numerical study of natural convective flow in an enclosure containing a heated cylinder and a cooled upper surface. A majority of the available studies [13–15] deal with natural convective flow and heat transfer around a circular cylinder kept inside an enclosure. There

* Corresponding author. Tel.: +91 512 2597429.
E-mail addresses: arkde@iitk.ac.in (A. Kumar De), amaresh@iitk.ac.in (A. Dalal).

0017-9310/$ - see front matter © 2006 Elsevier Ltd. All rights reserved.
doi:10.1016/j.ijheatmasstransfer.2006.04.020

Nomenclature

A	aspect ratio ($=H/L$)
a	side of the cylinder
g	gravitational acceleration
H	height of the enclosure
h	height of the cylinder from the bottom wall
J	Jacobian
k	thermal conductivity
L	length of the enclosure
l	local coordinate along the cylinder
Nu	Nusselt number
Pr	Prandtl number
P, Q	grid control functions
q_o	specified heat flux
Ra	Rayleigh number
T	dimensional temperature
Δt	time increment
U, V	dimensionless contravariant velocity components in ξ- and η-direction
u, v	velocity components in x- and y-direction
x, y	Cartesian coordinates

Greek symbols

v	dynamic viscosity
α_f	thermal diffusivity
β_f	volumetric thermal expansion coefficient
α, β, γ	geometric relations between coordinate systems
ξ, η	curvilinear coordinates
ω	vorticity
ψ	streamfunction
θ	dimensionless temperature
Φ	heat function

Subscripts

av	average
c	cold wall
h	hot wall
l	local
max	maximum
t, x, y, ξ, η	partial derivative relative to t, x, y, ξ, η, respectively

Superscripts

*	non-dimensional quantities
n	time stepping index

has been little study on the natural convection process with tilted heated cylinder inside an enclosure with cold side walls.

From application point of view, for electronic modules encapsulated inside a cabinet, the cooling effectiveness depends on the wall effect. It can be studied by modeling a heated square cylinder placed inside an enclosure. Natural convection in an enclosure containing a tilted heated cylinder is of interest in the present study. This configuration is different from the heated horizontal cylinder case from two different view points. Firstly, reduction in the blockage inside the enclosure facilitates the formation of convection rolls. Secondly, the more streamlined shape of the cylinder favors the development of the boundary layer and more interestingly its interaction with the core fluid. This configuration has been extensively studied for two different thermal extremities described in the next section. Flow and heat transfer has been analyzed using convection roll patterns and temperature variation inside the enclosure. Numerical visualization of heat transfer has been attempted by the concept of heatlines.

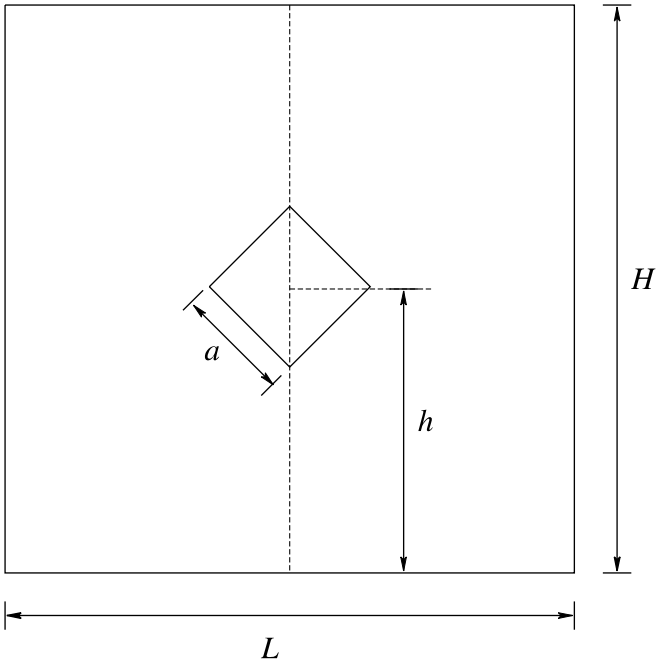

Fig. 1. Geometry describing the physical problem.

2. Problem specification

Fig. 1 shows the geometry in which natural convective heat transfer is studied in the present work. It consists of an enclosure having insulated horizontal and cold vertical walls containing air ($Pr = 0.71$) as working fluid. A heated cylinder is placed at the center of the enclosure in a prismatic orientation.

Only one half of the geometry is chosen as the computational domain due to symmetry. Fig. 2 shows the computa-

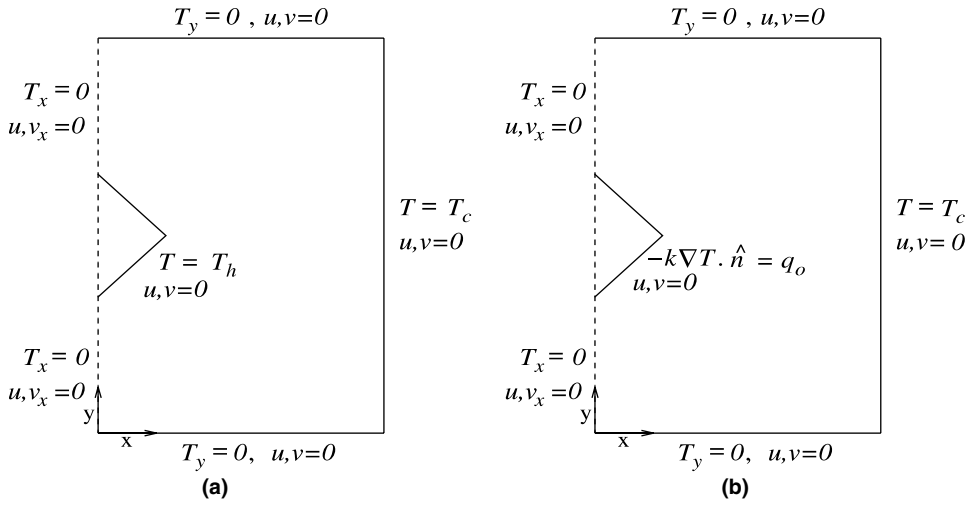

Fig. 2. Computational model with boundary conditions (a) Case 1, (b) Case 2.

tional domain with appropriate boundary conditions. Two modes of heating is considered in the present study. Case 1 refers to the situation with isothermal cylinder (Fig. 2(a)) while Case 2 refers to the uniform heat flux (Fig. 2(b)).

3. Mathematical formulation

The equations governing fluid flow and heat transfer in two dimension are written below in streamfunction-vorticity formulation. These equations are obtained after invoking Boussinesq approximation

$$\omega_t + (u\omega)_x + (v\omega)_y = \nu(\omega_{xx} + \omega_{yy}) + g\beta T_x \tag{1}$$

$$T_t + (uT)_x + (vT)_y = \alpha(T_{xx} + T_{yy}) \tag{2}$$

$$\psi_{xx} + \psi_{yy} = -\omega \tag{3}$$

$$u = \psi_y, \quad v = -\psi_x \tag{4}$$

Boundary conditions applicable in the present study are shown in the figure describing the physical problem (Fig. 2). The following scales are taken for the normalization of the above equations

$$x^* = \frac{x}{H}, \quad y^* = \frac{y}{H}, \quad u^* = \frac{uH}{\alpha}, \quad v^* = \frac{vH}{\alpha}, \quad t^* = \frac{\alpha t}{H^2},$$

$$\omega^* = \frac{\omega H^2}{\alpha}, \quad \psi^* = \frac{\psi}{\alpha}, \quad \theta = \frac{T - T_c}{T_h - T_c} \text{ for Case 1 and}$$

$$\theta = \frac{k(T - T_c)}{q_o H} \text{ for Case 2} \tag{5}$$

Using general curvilinear coordinates $x = x(\xi,\eta)$, $y = y(\xi,\eta)$, the set of non-dimensional transformed equations are

$$\omega_t + \frac{1}{J}((U\omega)_\xi + (V\omega)_\eta) = Pr\nabla^2\omega + \frac{1}{J}RaPr(y_\eta\theta_\xi - y_\xi\theta_\eta) \tag{6}$$

$$\theta_t + \frac{1}{J}((U\theta)_\xi + (V\theta)_\eta) = \nabla^2\theta \tag{7}$$

$$\nabla^2\psi = -\omega \tag{8}$$

$$u = \frac{1}{J}(-x_\eta\psi_\xi + x_\xi\psi_\eta), \quad v = \frac{1}{J}(-y_\eta\psi_\xi + y_\xi\psi_\eta) \tag{9}$$

where $U = y_\eta u - x_\eta v$ and $V = -y_\xi u + x_\xi v$ are the contravariant velocity components in ξ- and η-directions

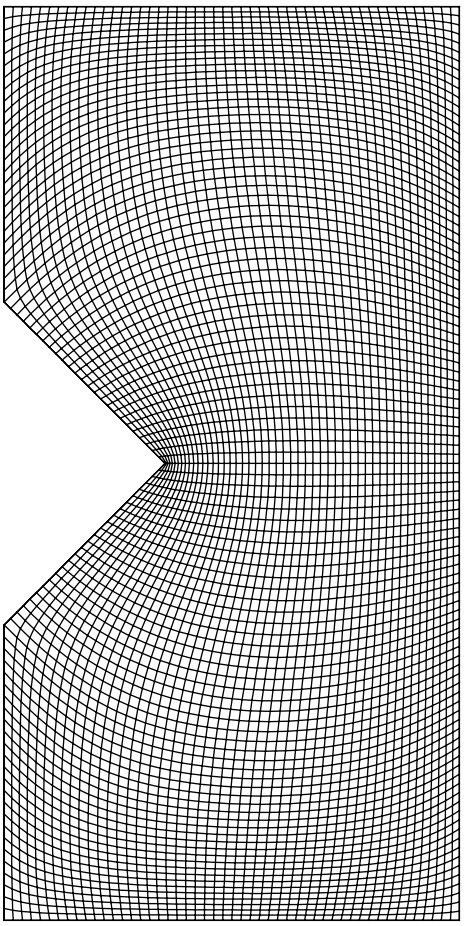

Fig. 3. A typical numerical grid (51×101) for $A = 1$, $h = 0.5$.

respectively and J is the Jacobian of the transformation defined as $J = x_\xi y_\eta - y_\xi x_\eta$. The Laplacian of a generic scalar ϕ in the transformed plane is given as

$$\nabla^2\phi = \frac{1}{J^2}(\alpha\phi_{\xi\xi} + \beta\phi_{\xi\eta} + \gamma\phi_{\eta\eta}) + \frac{1}{J^3}[(-y_\eta A + x_\eta B)\phi_\xi + (y_\xi A - x_\xi B)\phi_\eta] \quad (10)$$

where $\alpha = x_\eta^2 + y_\eta^2$, $\gamma = x_\xi^2 + y_\xi^2$, $\beta = -2(x_\xi x_\eta + y_\xi y_\eta)$, $A = \alpha x_{\xi\xi} + \beta x_{\xi\eta} + \gamma x_{\eta\eta}$ and $B = \alpha y_{\xi\xi} + \beta y_{\xi\eta} + \gamma y_{\eta\eta}$.

4. Numerical technique

In this section numerical method adopted in the present study is discussed.

4.1. Grid generation

In the present study curvilinear body-fitted grids have been generated by solving Poisson equations for the curvilinear coordinates given as

$$\nabla^2\xi = P(\xi,\eta) \quad (11)$$

$$\nabla^2\eta = Q(\xi,\eta) \quad (12)$$

where P and Q are the control functions required to retain the desired grid density in the domain. The above two equations can be written as below with the physical coordinates as the dependent variables

$$\alpha x_{\xi\xi} + \beta x_{\xi\eta} + \gamma x_{\eta\eta} + J^2(Px_\xi + Qx_\eta) = 0 \quad (13)$$

$$\alpha y_{\xi\xi} + \beta y_{\xi\eta} + \gamma y_{\eta\eta} + J^2(Py_\xi + Qy_\eta) = 0 \quad (14)$$

In the present study control functions are used to maintain a desired grid density near the cylinder alleviating the problem of poor grid distribution near a concave surface using elliptic grid generation technique [16]. Eqs. (13) and (14) are solved by SOR method. All the derivatives are discretized using second order central difference scheme and the non-linearity is resolved through iterations. A typical generated grid is shown in Fig. 3.

Table 1
Comparison of present solutions using orthogonal grid with benchmark results

	a	b	c	d	$\frac{a-d}{a}\times 100$
(a) $Ra = 10^5$					
u_{max}	34.73 (0.855)	35.73 (0.857)	37.144 (0.855)	34.798 (0.850)	−0.196
v_{max}	68.59 (0.066)	69.08 (0.067)	68.91 (0.061)	68.340 (0.067)	0.364
ψ_{max}	9.612 (0.285, 0.601)			9.497 (0.283, 0.6)	1.2
$\overline{Nu}$	4.519	4.430	4.964	4.479	0.885
(b) $Ra = 10^6$					
u_{max}	64.63 (0.850)	68.81 (0.872)	66.42 (0.897)	66.948 (0.850)	−3.587
v_{max}	217.36 (0.0379)	221.8 (0.0375)	226.4 (0.0206)	219.663 (0.033)	−1.060
ψ_{max}	16.75 (0.151, 0.547)			16.455 (0.15, 0.55)	1.76
$\overline{Nu}$	8.799	8.754	10.39	9.312	−5.830

a: solution of Vahl Davis [1]; *b*: solution of Markatos and Perikleous [2]; *c*: solution of Hadjisophocleous et al. [9]; *d*: present solution on 61×61 grid.

Table 2
Comparison of present solutions using non-orthogonal grid with benchmark results

Pr		a	b	$\frac{a-b}{a}\times 100$
0.1	Nu_{av}	5.98493	5.97085	0.24
	Nu_{max}	8.6778 (0.45644)	8.6628 (0.44999)	0.17
	ψ_{min}	-9.68706×10^{-3} (0.78926, 0.178134)	-9.6679×10^{-3} (0.78511, 0.17677)	0.20
10	Nu_{av}	7.58013	7.59479	−0.19
	Nu_{max}	12.471 (0.17028)	12.606 (0.16666)	−1.08
	ψ_{min}	-1.662127×10^{-3} (0.57276, 0.319989)	-1.66587×10^{-3} (0.57409, 0.32409)	−0.23

a: solution of Demirdžić et al. [20]; *b*: present solution on 121×121 grid.

Table 3
Comparison of results at several grids for $Ra = 10^4$, $A = 1$ and $h = 0.5$

Grid	ψ_{max}	ψ_{min}	Nu_{max}*	% change	Nu_{av}*	% change	Nu_{av}**	% change
31×61	1.00014	−0.49277	15.6265		4.605		−2.271	
41×81	1.00012	−0.49091	17.2532	10.41	4.415	4.13	−2.206	2.86
51×101	1.00008	−0.48870	18.6184	7.91	4.255	3.62	−2.160	2.09
61×121	1.00006	−0.48811	19.8122	6.41	4.129	2.96	−2.122	1.76

* Hot wall.
** Cold wall.

4.2. Discretization technique and method of solution

The system of governing (Eqs. (6)–(9)) are solved by finite difference method in the transformed plane. All the spatial discretization is done with the second order central difference scheme except for the convective terms in the two transport equations which utilize standard QUICK scheme. A semi-implicit time integration scheme is adopted in the present study to advance the vorticity and temperature values in time. The vorticity transport equation and the energy equation both having non-linear convective terms are linearized as follows:

$$J\frac{\theta_{i,j}^{n+1}-\theta_{i,j}^{n}}{\Delta t}+\left(U^{n}\theta^{n+1}\right)_{i,j}+\left(V^{n}\theta^{n+1}\right)_{i,j}=J\left(\nabla^{2}\theta^{n+1}\right)_{i,j} \tag{15}$$

$$J\frac{\omega_{i,j}^{n+1}-\omega_{i,j}^{n}}{\Delta t}+\left(U^{n}\omega^{n+1}\right)_{i,j}+\left(V^{n}\omega^{n+1}\right)_{i,j}=JPr\left(\nabla^{2}\omega^{n+1}\right)_{i,j}+JRaPr\left(y_{\eta}\theta_{\xi}-y_{\xi}\theta_{\eta}\right)_{i,j}^{n+1} \tag{16}$$

The Laplacian in the above equations has already been written in Eq. (10). Discretized form of Eqs. (15) and (16) have been solved by SOR technique as they take a few iterations to converge due to the diagonal dominance. The system of linear equations arising from the discretization of the Poisson equation for the streamfunction is solved by the stabilized Bi-Conjugate Gradient Method (BiCGSTAB) [17]. This technique falls in the category of matrix free Krylov space based method which efficiently exploits the sparse structure of the coefficient matrix. Solution of all system of linear equations are terminated when l_2 norm of error of the equations reach a pre-assigned value ϵ which is 10^{-5} for two transport equations and 10^{-6} for the Poisson equation. A time increment $\Delta t = 10^{-5}$ has been used for $Ra = 10^3$–10^5 and 5×10^{-6} for $Ra = 10^6$.

The definition of vorticity has been used to compute boundary vorticity with partial derivatives of the velocities are discretized by second order accurate one-sided formulas. This is as follows:

$$\omega_b=(v_x-u_y)_b=\left[\frac{1}{J}\left(y_\eta v_\xi-y_\xi v_\eta+x_\eta u_\xi-x_\xi u_\eta\right)\right]_b$$

Local Nusselt number at the right wall and on the cylinder has been calculated by the following expression [18]:

$$\text{Side wall:}\quad Nu_l=\frac{1}{J\sqrt{\alpha}}\left(\alpha T_\xi-\gamma T_\eta\right)$$

$$\text{Cylinder wall:}\quad Nu_l=\frac{-1}{J\sqrt{\alpha}}\left(\alpha T_\xi-\gamma T_\eta\right)$$

4.3. Heatline

In analogy to the streamfunction in two-dimension, heatfunction $\Phi(x,y)$ is defined in non-dimensional from as [19]

$$-\Phi_x=v\theta-\theta_y \tag{17}$$

$$\Phi_y=u\theta-\theta_x \tag{18}$$

Elimination of the gradient terms by cross differentiation of the above two equations, yields a conduction type equation

$$\Phi_{xx}+\Phi_{yy}=(u\theta)_y-(v\theta)_x \tag{19}$$

In the transformed plane, definition equations of heatlines take the form

$$-\Phi_\xi=V\theta-\frac{1}{J}\left(\gamma\theta_\eta+\frac{\beta}{2}\theta_\xi\right) \tag{20}$$

$$\Phi_\eta=U\theta-\frac{1}{J}\left(\alpha\theta_\xi+\frac{\beta}{2}\theta_\eta\right) \tag{21}$$

and the conduction-type equation becomes

$$\nabla^2\Phi=S \tag{22}$$

where $S=\frac{1}{J}\left[-(u\theta)_\xi x_\eta+(u\theta)_\eta x_\xi-(v\theta)_\xi y_\eta+(v\theta)_\eta y_\xi\right]$ and the Laplacian in the transformed plane has been given in Eq. (10). Eq. (22) has been solved for the heatfunction with the following boundary conditions derived from its definitions (Eq. (20) or (21)). In deriving the boundary conditions, the bottom left corner of the enclosure has been taken as the reference point where the value of heatfunction is zero

$$\Phi(x,0)=0,\quad 0\leqslant x\leqslant\frac{L}{2}$$

$$\Phi\left(\frac{L}{2},y\right)=-\int_0^y\theta_x\,\mathrm{d}y=-\int_0^y\frac{1}{J}(\theta_\xi y_\eta-\theta_\eta y_\xi)\,\mathrm{d}\eta,\quad 0\leqslant y\leqslant H$$

$$\Phi(0,y)=0,\quad 0\leqslant y\leqslant h-\frac{a}{\sqrt{2}}$$

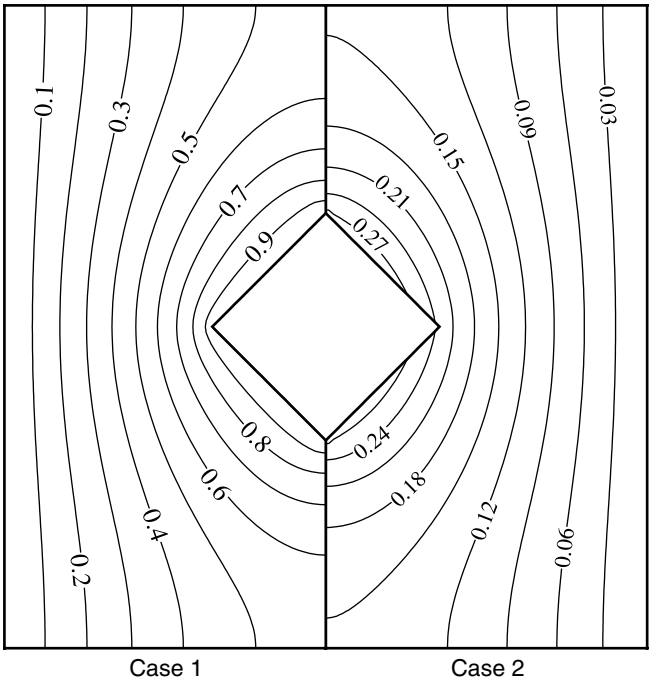

Fig. 4. Isotherms for pure conduction, $A = 1$, $h = 0.5$.

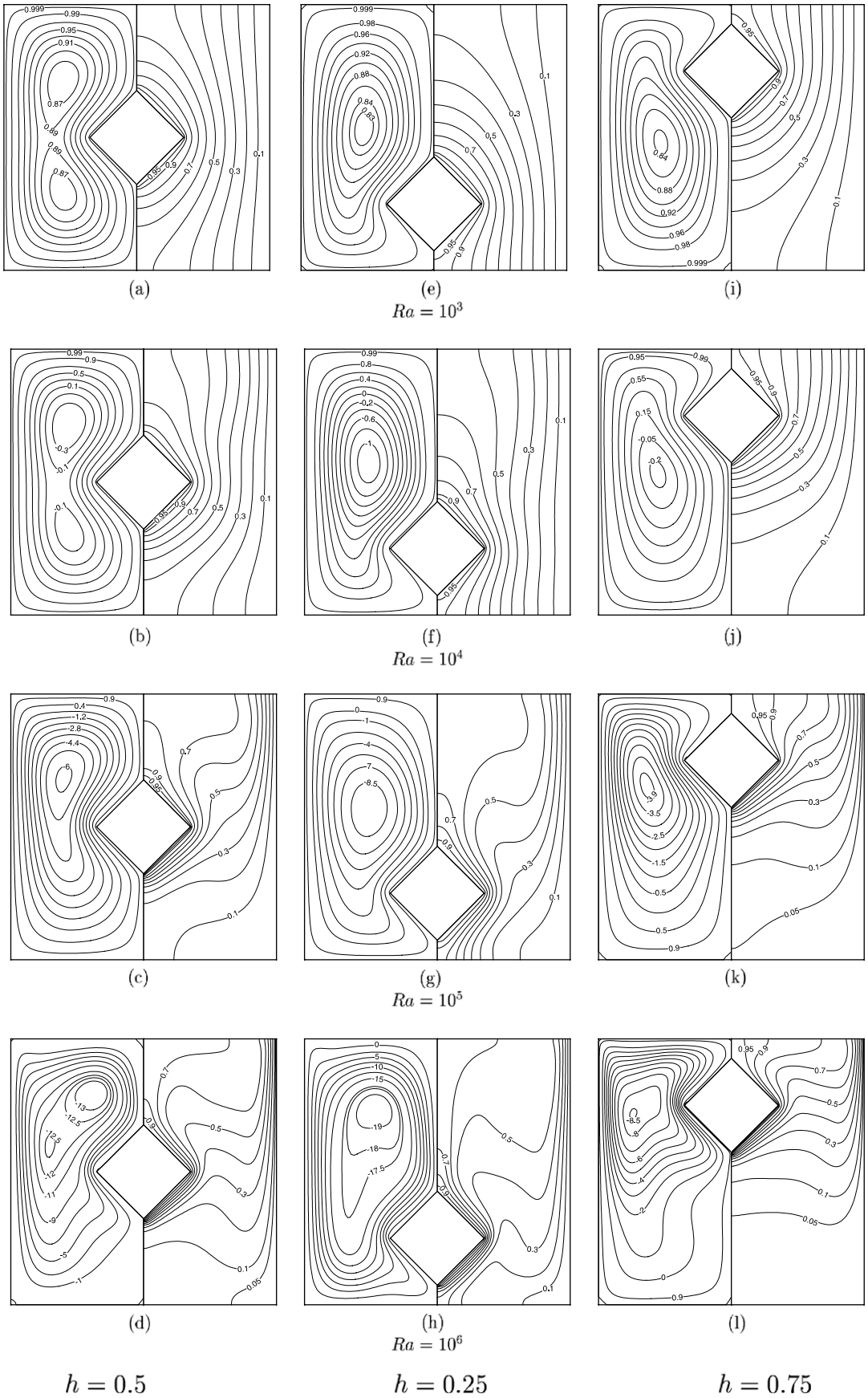

Fig. 5. Streamlines and isotherms for Case 1, $A = 1$.

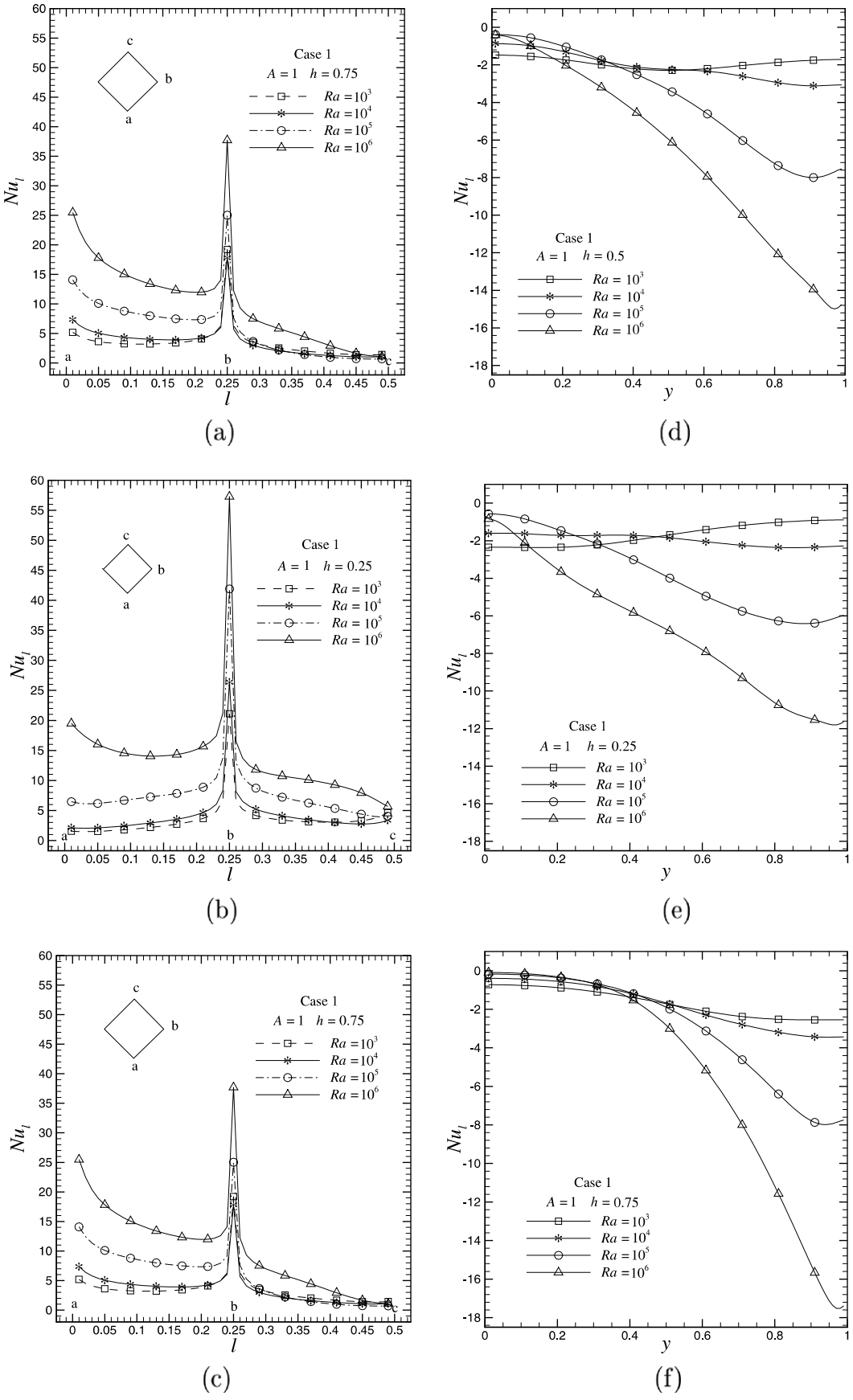

Fig. 6. Local Nusselt number distribution for Case 1, $A = 1$.

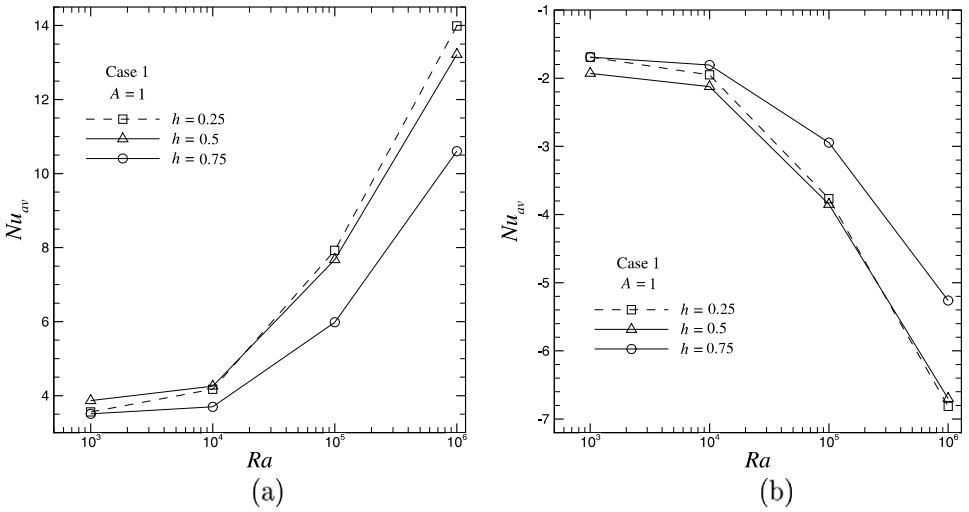

Fig. 7. Average Nusselt number for Case $A = 1$: (a) on the cylinder, (b) on the side wall.

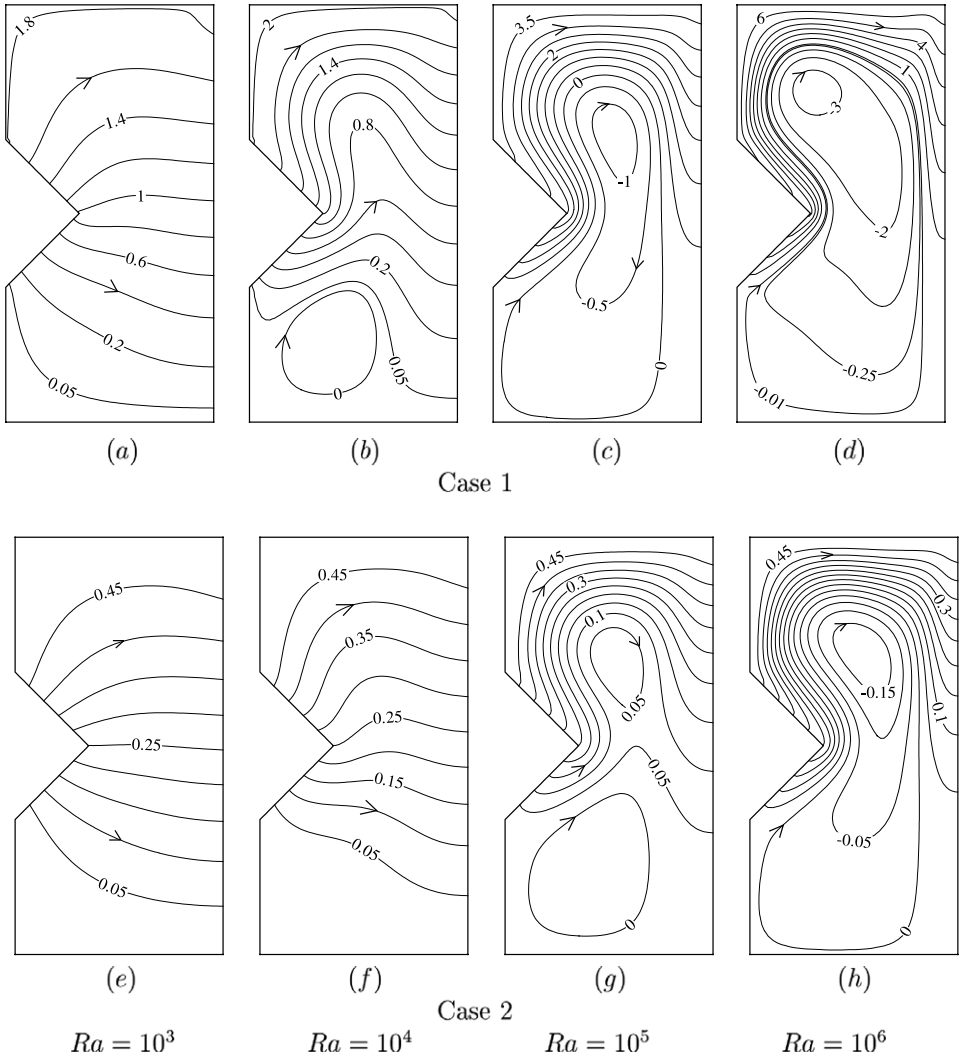

Fig. 8. Heatlines for $A = 1$, $h = 0.5$.

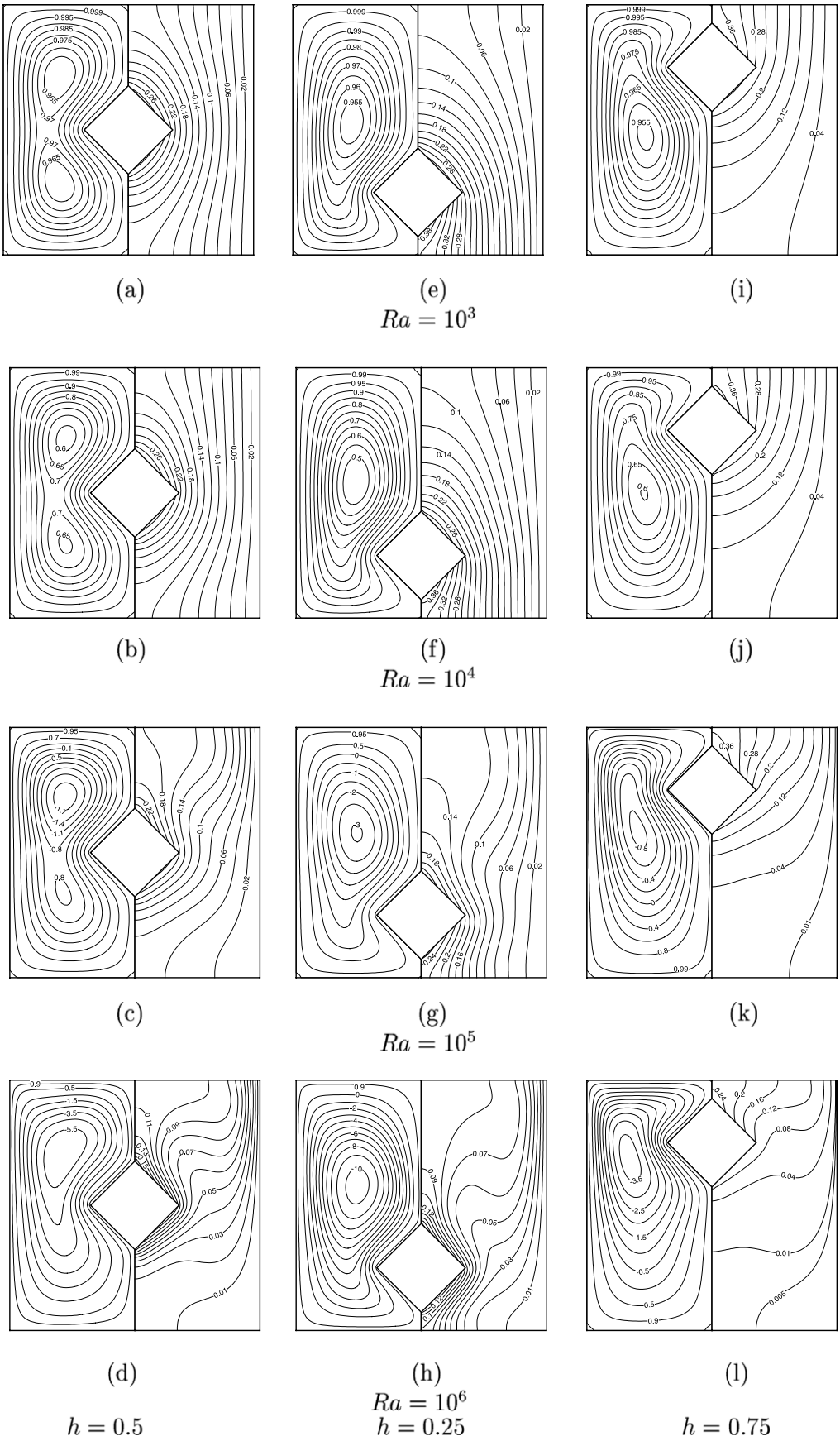

Fig. 9. Streamlines and isotherms for Case 2, $A = 1$.

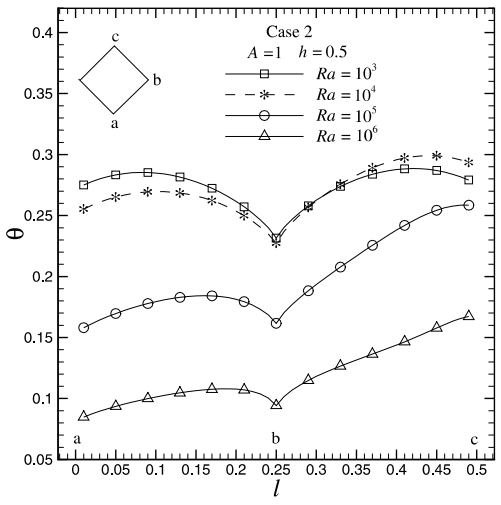

(a)

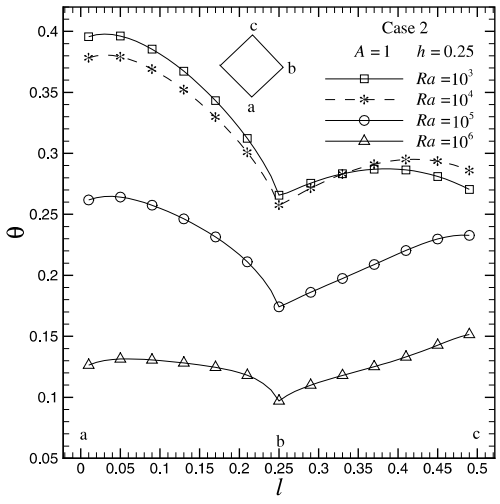

(b)

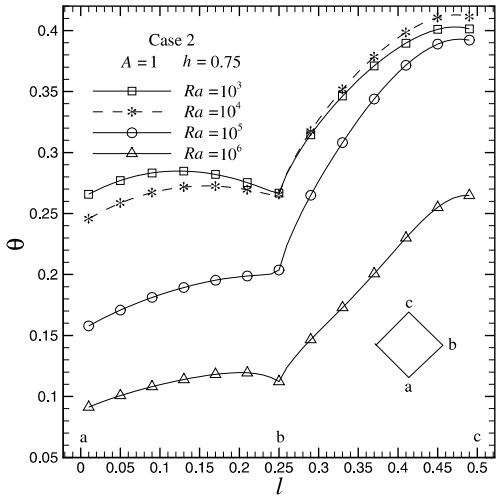

(c)

Fig. 10. Local surface temperature distribution on the cylinder for Case 2, $A = 1$.

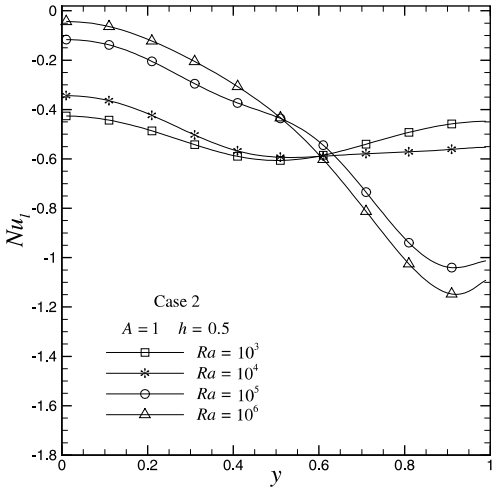

(a)

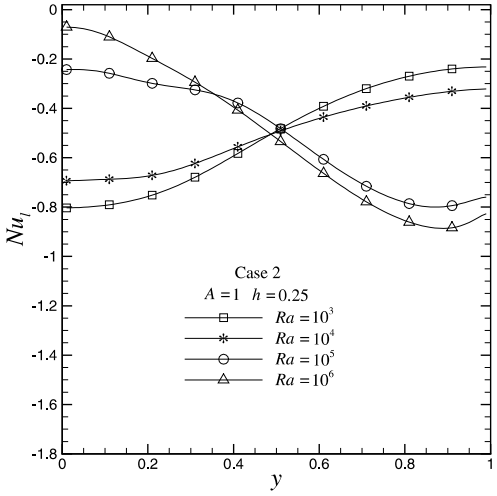

(b)

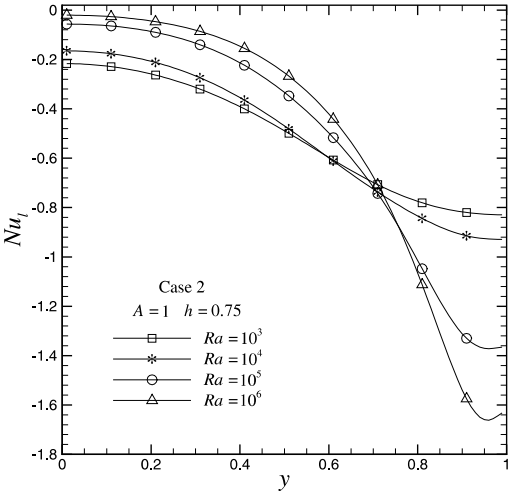

(c)

Fig. 11. Local Nusselt number distribution on the side wall for Case 2, $A = 1$: (a) $h = 0.5$, (b) $h = 0.25$, (c) $h = 0.75$.

$$\Phi(0,y) = -\int_{h-\frac{a}{\sqrt{2}}}^{h+\frac{a}{\sqrt{2}}} \frac{1}{J}\left(\alpha\theta_\xi + \frac{\beta}{2}\theta_\eta\right)\mathrm{d}\eta, \quad h-\frac{a}{\sqrt{2}} \leqslant y \leqslant h+\frac{a}{\sqrt{2}}$$

$$\Phi(0,y) = \Phi\left(0, h+\frac{a}{\sqrt{2}}\right), \quad h+\frac{a}{\sqrt{2}} \leqslant y \leqslant H$$

$$\Phi(x,H) = \Phi(0,H), \quad 0 \leqslant x \leqslant \frac{L}{2}$$

4.4. Computer code validation

The computer code developed for the present study is validated for natural convection in a differentially heated cavity both for an orthogonal and non-orthogonal configurations at different Rayleigh numbers. Table 1 shows the comparison with the numerical results of Vahl Davis [1] and others [2,9] for the orthogonal configuration where results match closely for $Ra = 10^5$ while they are acceptable range for $Ra = 10^6$. An excellent match has been found for the non-orthogonal case with Demirdžić et al. [20], as can be seen from Table 2, where difference only goes beyond 1% for Nu_{max} at $Pr = 10$.

4.5. Grid independence test

To see the effect of size of the numerical grid, a thorough grid independence test has been carried out for Case 1 with $Ra = 10^4$. Four levels of grids namely, 31×61, 41×81, 51×101, 61×121 have been tested and the results are tabulated in Table 3. It has been observed that as the grid is refined, variation in the results between two successive grids decreases. For the two finest level of grids, difference in Nu_{max} on the cylinder is 6.41% while Nu_{av} changes only 2.96%. However, variation in Nu_{av} on the side wall remains below 2% for the two finest grid levels. This has lead us to use 51×101 for $A = 1$, 25×101 for $A = 2$, 61×101 for $A = 0.5$ in all subsequent calculations considering relative cost of computation with achievable accuracy.

5. Results and discussion

The results are presented for a number of cases corresponding to two different thermal boundary conditions, geometric aspect ratio and the position of the heated cylinder. The basic features of flow and heat transfer are analyzed with the help of isotherms and the streamline patterns. Heatlines are also shown to further investigate the mode of heat transfer. Local and average Nusselt numbers on the isothermal surfaces are plotted to evaluate the local and overall heat transfer process.

5.1. Basic flow and heat transfer features

Fig. 4 shows isotherms for the pure conduction problem. We first take up Case 1. As it can be seen from Fig. 5, temperature distribution inside the enclosure deviates significantly from the pure conduction case at higher Rayleigh numbers emphasizing the prevalence of buoyancy induced convection. Since the cylinder is kept heated, the hot fluid is pumped in by the cylinder and rises upward near the vertical mid plane of the enclosure due to thermal expansion. This hot fluid moves horizontally toward corners after impinging on the roof. Finally, the colder and thus denser fluid descends along the cold side walls as it comes in contact with cooled fluid away from the cylinder. As Rayleigh number increases, isotherms are distorted and the formation of the thermal boundary layer on the cylinder surface from the bottom to the top and on the enclosure-side wall from the top to the bottom is prominent. This feature is identical for all the positions of the cylinder and leads to a stable stratification at the core of the enclosure at high Rayleigh number. The denser streamlines near the enclosure wall and the cylinder and relative absolute values show the stronger convective flow at higher Rayleigh numbers. While the flow pattern changes from a bi-cellular to an uni-cellular form at high Rayleigh number for $h = 0.5$, no such behavior is found for other two positions of the cylinder. For $h = 0.75$, flow is primarily confined to the upper half of the enclosure leaving a lump of cold fluid at the bottom half showing poorer mixing compared to the other two cases. The presence of high temperature gradient in both the isothermal walls at high Rayleigh number leads to higher local Nusselt number as is evident from Fig. 6. A sharp peak in the local Nusselt number is visible (Fig. 6(a)–(c)) which occurs due to the sharp variation of the metric coefficients at the tip of the cylinder leading to a high temperature gradient. On the isothermal cold wall (Figs. 6(d)–(f)) local Nusselt number hardly varies for lower Rayleigh numbers due to the absence of a prominent thermal boundary layer. However, at higher Rayleigh

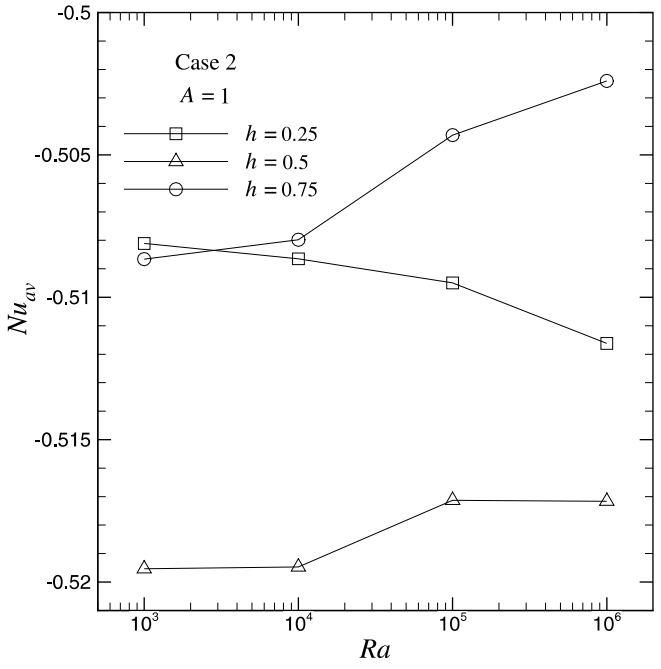

Fig. 12. Average Nusselt number on the side wall for Case 2, $A = 1$.

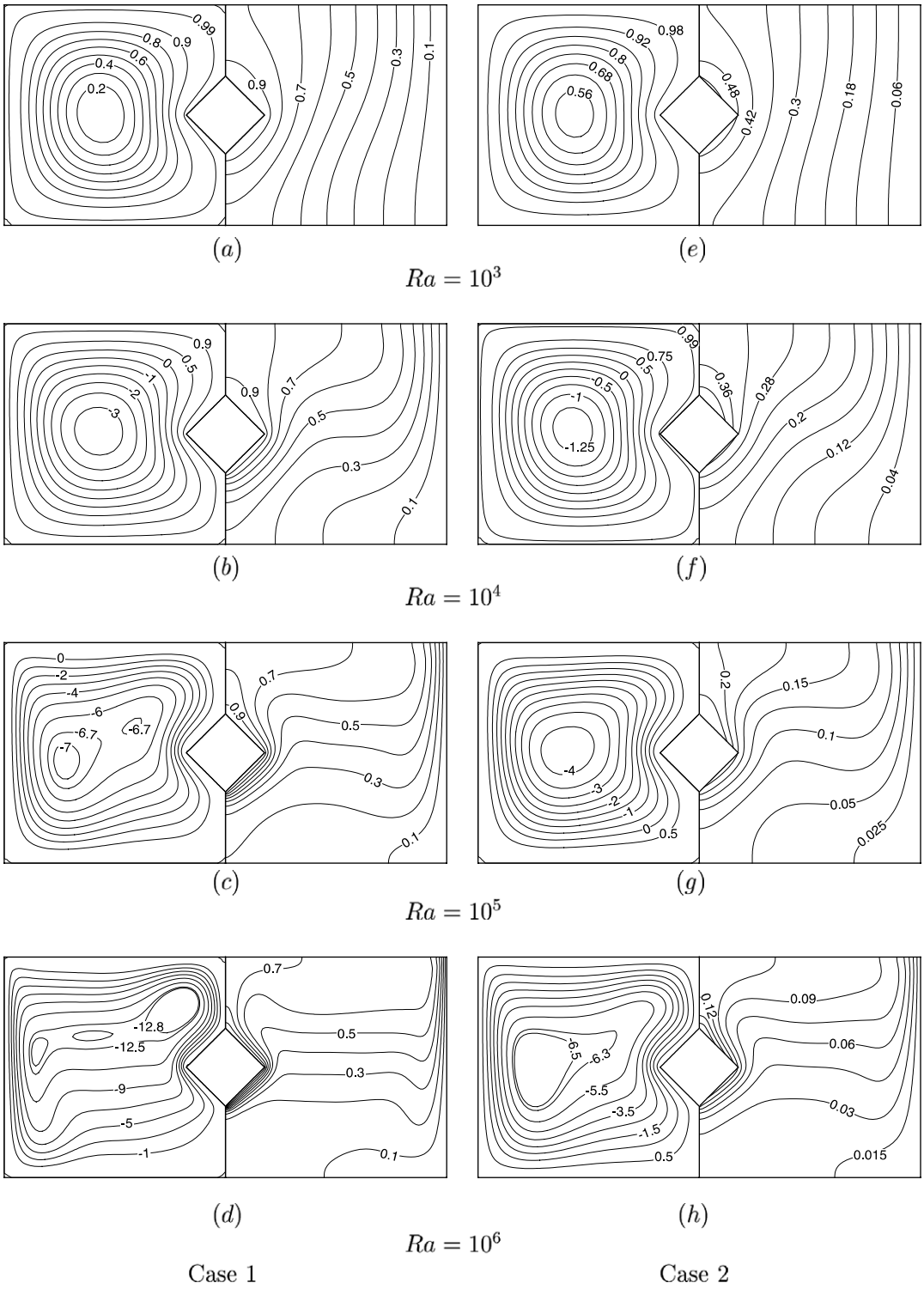

Fig. 13. Streamlines and isotherms for $A = 0.5$.

numbers Nu_l increases in absolute value in the direction of development of the thermal boundary layer. Note that Nu_l is negative in Figs. 6(d)–(f) as heat is released by the enclosure through the cold wall. Average Nusselt number on the cylinder and the side wall are plotted against Rayleigh number for different cylinder positions in Fig. 7(a) and (b) respectively. Heat exchange between fluid and the walls enhances for the higher Rayleigh numbers as absolute value of Nu_{av} increases with Rayleigh number. Nu_{av}–Ra curves change slowly for $Ra \leqslant 10^4$ and almost linearly for $Ra > 10^4$. Nu_{av} for $h = 0.75$ is quantitatively lesser compared to $h = 0.25$ and 0.5 owing to poor mixing and heat transfer from the isothermal walls, a fact already been discussed in accordance with Fig. 5. This underlines the effect

of position of the cylinder in the overall heat transfer process.

Heatlines, the path of heat transport is shown in Fig. 8 for two different thermal boundary conditions. There are certain similar characteristics between the streamlines and the heatlines. Analogous to the streamlines, heatlines also start and stop at boundaries or circulate as vortex. Its value is of relativity, depending on the reference value assumed in the calculation. As depicted in the figure, heat transfer is conduction dominated at lower Rayleigh numbers which is evident from the almost straight and evenly spaced heatlines. The arrow in the figure shows the direction of heat transport. As Rayleigh number increases, heatlines bend toward the upper half of the enclosure owing to the strong convection effect leading to non-uniform distribution of heat flux on the isothermal surfaces. This strengthens the occurrence of convection dominated heat transfer mechanism at higher Rayleigh numbers. The crowded pattern of the heatlines in the upper half of the enclosure confirms that flow occurs along the walls leaving a stagnant stratified pool of fluid in the core. The non-uniformity of the heatflux manifests in higher temperature gradient on the isothermal walls leading to higher local Nusselt number, a fact already been observed. The smaller values of heatfunctions in case of uniform heat flux (Case 2) signifies the attenuation of heat transfer between the isothermal walls. The dominance of convection over conduction is brought forth at relatively higher Rayleigh numbers as compared to Case 1. Moreover, the presence of a thin thermal boundary layer and non-uniform distribution of heat flux on the isothermal surfaces and confinement of heat carrying fluid in the upper half of the enclosure are less evident for Case 2.

5.2. Effect of thermal boundary condition

Although the basic flow and heat transfer features do not change significantly for the two different heating

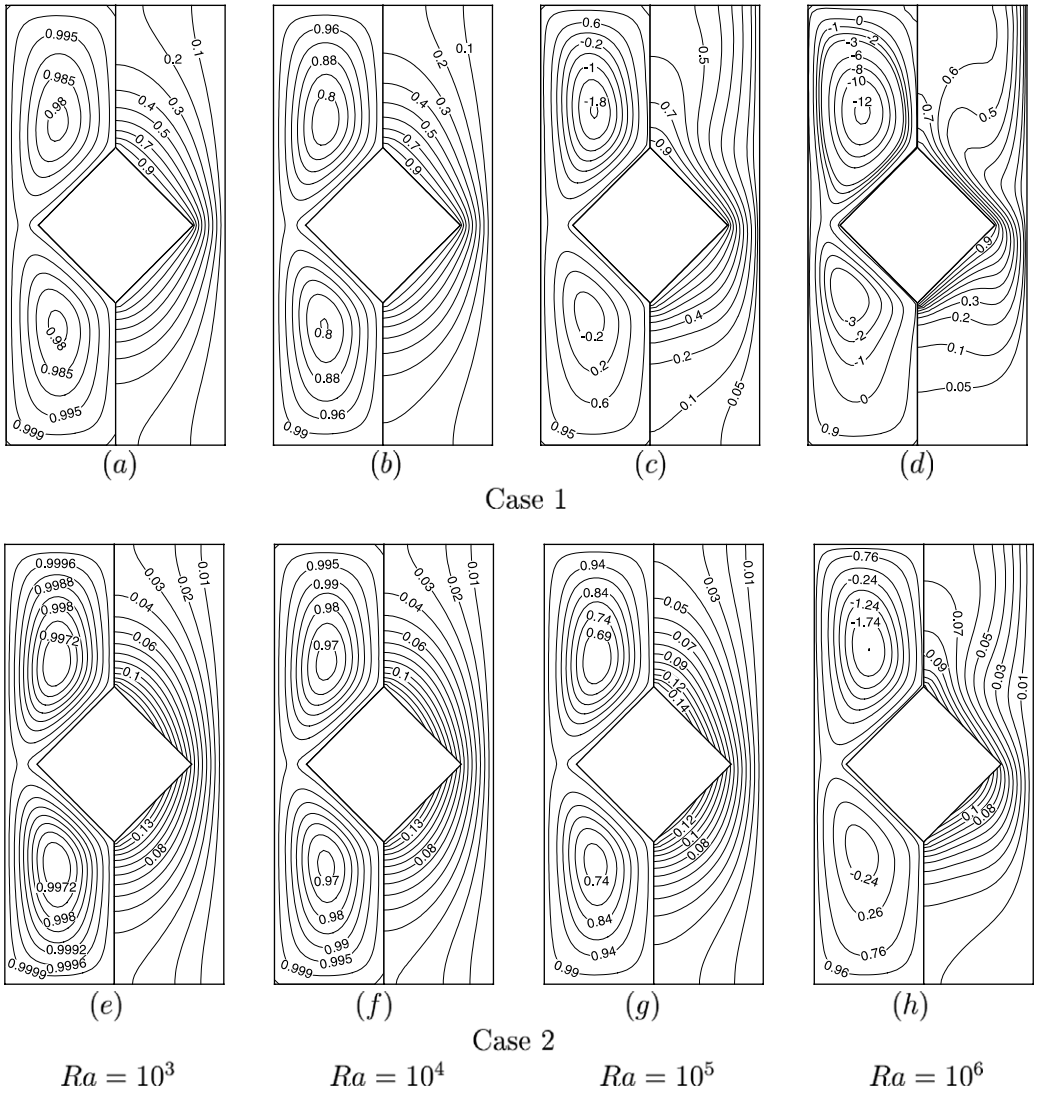

Fig. 14. Streamlines and isotherms for $A = 2$.

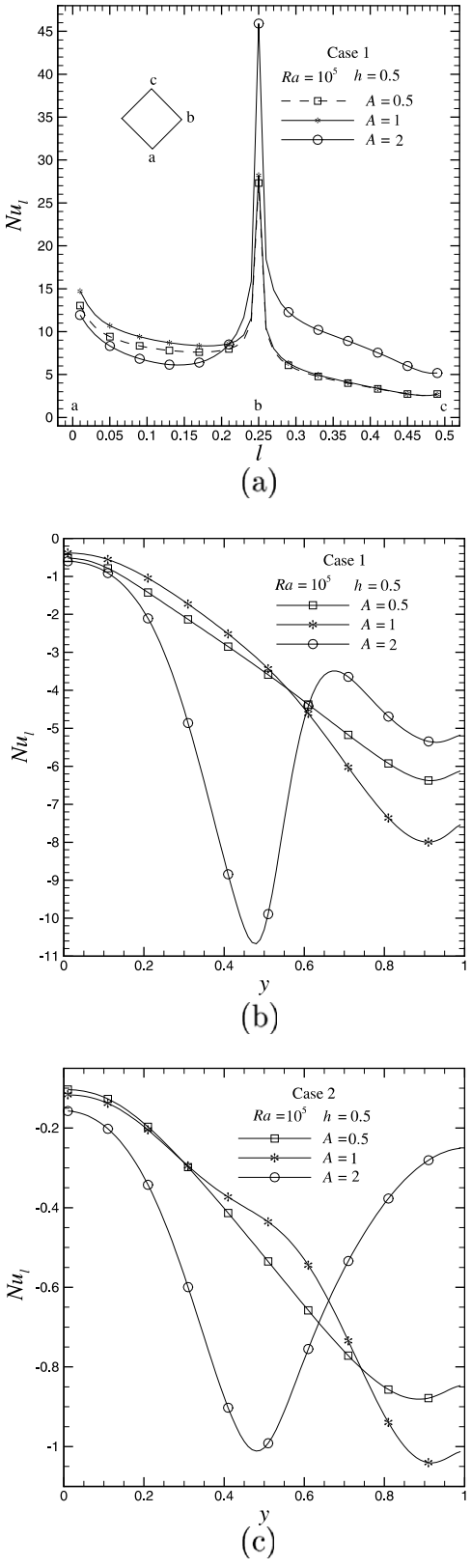

Fig. 15. Local Nusselt number distribution with $h = 0.5$ for Case 1 (a) cylinder, (b) side wall and Case 2 (c) side wall.

modes, distribution of isotherm (Fig. 9) is quantitatively different for Case 2. In the absence of any perceivable thermal boundary layer, vertical stratified layers are seen even at $Ra = 10^5$ for Case 2 with $h = 0.25$ and $h = 0.5$. As Rayleigh number increases, heated fluid layers are observed to exist close to the cylinder showing lesser heat transfer from the cylinder in case of constant heat flux heating. Also dominance of convection at higher Rayleigh numbers is less evident for this type of heating as can be seen from numerical values of ψ. Fig. 10 depicts the local temperature distribution on the cylinder. Temperature distribution along the cylinder is almost symmetric about its tip at lower Ra while it becomes increasingly asymmetric with increase in Ra owing to better accumulation of the fluid in the converging passage near the lower half of the cylinder for $h = 0.5$. The narrow passage near the adiabatic horizontal wall prevents the fluid to come in contact with the cylinder leading to higher temperature on the cylinder face close to the wall for $h = 0.25$ and 0.75. At higher Rayleigh numbers temperature drops on the cylinder surface showing better heat removal with minimum temperature occurring at the highest Rayleigh number. Local Nusselt number distribution on the cold wall is shown in Figs. 6(d)–(f) and 11 for the two cases with different h. It is clear that due to ineffective heat transfer for Case 2 heating, local Nusselt number hardly changes as compared to the Case 1 which is also confirmed by the average Nusselt number plots (Figs. 7(b) and 12) for the two cases at different Rayleigh numbers. At smaller Rayleigh numbers local Nusselt number does not change significantly along the side wall while at higher Rayleigh numbers, due to the higher temperature gradient at the upper half of the enclosure Nusselt number decreases in the direction of the cold fluid descend.

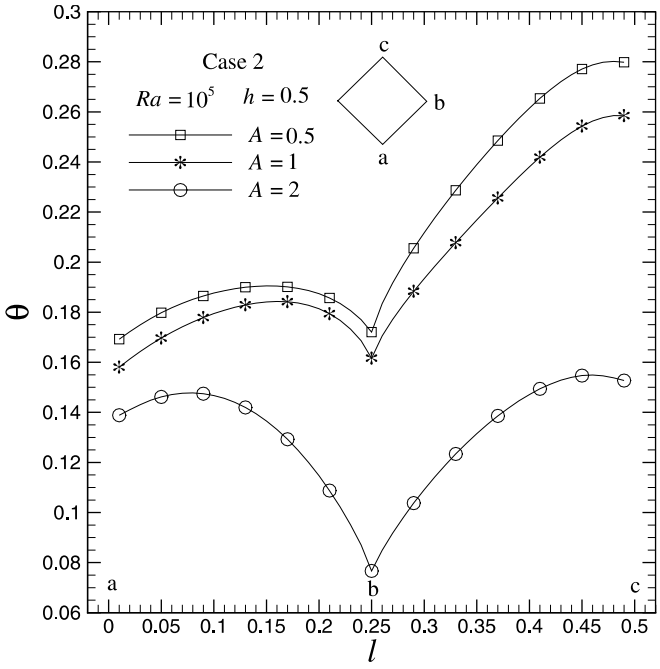

Fig. 16. Local surface temperature distribution on the cylinder for Case 2, $h = 0.5$.

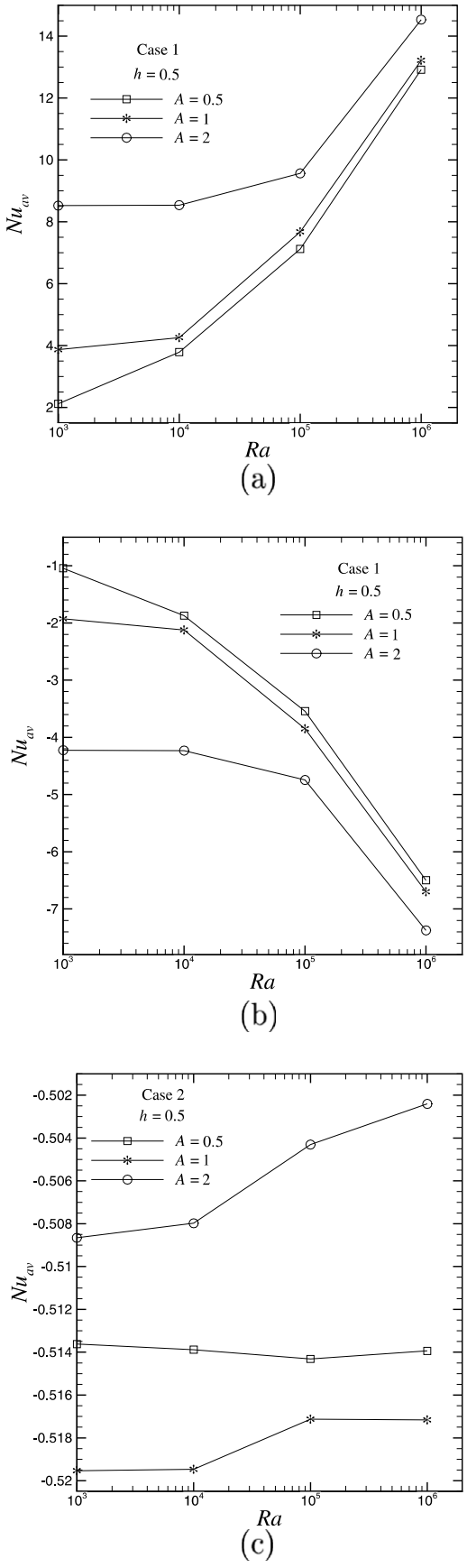

Fig. 17. Average Nusselt number distribution for different aspect ratios, $h = 0.5$: Case 1 (a) cylinder, (b) side wall and Case 2 (c) side wall.

5.3. Effect of aspect ratio

In order to assess the effect of geometric aspect ratio of the enclosure, three different configurations, $A = 0.5$, 1 and 2 have been studied in the present work. Figs. 13 and 14 show the streamlines and isotherms for $A = 0.5$ and 2 respectively. For the highest aspect ratio, flow is observed to be bi-cellular at all Rayleigh numbers showing existence of multicellular natural convection loops in tall vertical enclosures. At the lowest aspect ratio, due to the lowest blockage imposed by the cylinder, streamlines and isotherms closely resemble the flow features of the differentially heated vertical cavity nullifying to some extent the presence of the heated cylinder. The pattern of convective cells are found to be quite similar for the two lowest aspect ratios. The distribution of isotherms is distinctively different for all the three aspect ratios. At $A = 2$, isotherms are concentric in shape and varies radially at low Rayleigh number. Almost stagnant vertical stratified layers switches to horizontal layers with the increase in Rayleigh number for $A = 0.5$ showing that the convecting fluid remains close to the isothermal surfaces and heat transfer is confined there. Local Nusselt number distribution on the cylinder (Fig. 15(a)) remains almost identical for different aspect ratio with the maximum Nusselt number, occurring at the tip, increases as the side wall moves close to the cylinder. Local Nusselt number on the cold wall as shown in Figs. 15(b) and (c) decreases monotonically along the surface for $A = 0.5$ and 1 but is different for $A = 2$. This happens because as aspect ratio increases, the cold wall comes closer to the cylinder and the descending cold fluid is made to pass through a small gap leading to a high temperature gradient which shows up as a peak in the local Nusselt number distribution. This is also the reason why temperature on the cylinder for Case 2 is different for $A = 2$ as compared to $A = 0.5$ and 1 which are quite similar (Fig. 16). Average Nusselt number on the cylinder, the side wall for Case 1 and only on the side wall for Case 2 are shown in Fig. 17(a)–(c) respectively. The difference in absolute value of average Nusselt number among aspect ratios decreases with increase in Rayleigh number for Case 1 indicating strong buoyancy induced convection overwhelms geometric features. However, Nu_{av} does not change significantly for different aspect ratios owing to inferior heat transfer as already observed for Case 2.

6. Conclusions

A numerical study has been carried out for natural convective flow and heat transfer around a tilted heated cylinder kept in an enclosure with cooled side walls. The numerical code thus developed has been validated against the benchmark solutions. Detailed parametric study involving the effects of thermal boundary conditions, location of the heated cylinder and geometric aspect ratio have been reported. The concept of heatfunction has been employed to identify the path of heat transport. Based on

the observations made during the study, the authors propose the following:

- Constant wall temperature heating is efficient in comparison to the constant wall heat flux mode in view of overall heat transfer for the present physical situation.
- Location of the heated cylinder does not play an important role which is confirmed by both local and average Nusselt numbers for Case 1.
- For geometry with higher aspect ratio, flow is essentially multicellular at all Rayleigh numbers. Due to the availability of small passage for the ascending and descending fluid, location of the cylinder becomes important leading to different trend in the local Nusselt number distribution.
- Change in overall heat transfer for different aspect ratios is found in the lower Rayleigh numbers while it diminishes as Rayleigh number is increased for Case 1.

Acknowledgements

The authors acknowledge the computational facilities extended by the CFD Laboratory of the Mechanical Engineering Department at IIT Kanpur.

References

[1] G. de Vahl Davis, Natural convection of air in a square cavity: a benchmark numerical solution, Int. J. Numer. Methods Fluids 3 (1983) 249–264.
[2] N.C. Markatos, K.A. Perikleous, Laminar and turbulent natural convection in an enclosed cavity, Int. J. Heat Mass Transfer 27 (5) (1984) 755–772.
[3] S. Ostrach, Natural convection in enclosures, J. Heat Transfer 50th Anniversary Issue 110 (4-B) (1988) 1175–1190.
[4] P.H. Oosthuizen, P.F. Monaghan, Free convective flow in a vertical non-rectangular cavity with a cooled flat upper surface, Natural/Forced Convection and Combustion Simulation (1992) 191–208.
[5] P.H. Oosthuizen, Free convective flow in an enclosure with a cooled inclined upper surface, Comput. Mech. 14 (1994) 420–430.
[6] M.M. Ganzarolli, L.F. Milanez, Natural convection in rectangular enclosures heated from below and symmetrically cooled from the sides, Int. J. Heat Mass Transfer 38 (1995) 1063–1073.
[7] W. Chmaissem, D. Daguenet, Numerical study of the natural convection of Boussinesq equations in parallelepipedal cavities with isothermal walls and heated from two sides: influence of wall conditions, Energy Convers. Manage. 40 (1999) 1041–1056.
[8] A. Dalal, M.K. Das, Laminar natural convection in an inclined complicated cavity with spatially variable wall temperature, Int. J. Heat Mass Transfer 48 (2005) 3833–3854.
[9] G.V. Hadjisophocleous, A.C.M. Sousa, J.E.S. Venart, Prediction of transient natural convection in enclosures of arbitrary geometry using a nonorthogonal numerical model, Numer. Heat Transfer 13 (1988) 373–392.
[10] D.W. Larson, D.K. Gartling, W.P. Schimmel, Natural convection studies in nuclear spent-fuel shipping casks: computation and experiment, J. Energy 2 (3) (1993).
[11] D.G. Roychowdhury, S.K. Das, T.S. Sundararajan, Numerical simulation of natural convective heat transfer and fluid flow around a heated cylinder inside an enclosure, Heat Mass Transfer 38 (2002) 565–576.
[12] A.R. Elepano, P.H. Oosthuizen, Free convective heat transfer from a heated cylinder in an enclosure with a cooled upper surface, in: L.C. Wrobel, C.A. Brabbia, A.J. Nowak (Eds.), Advanced Computational Methods in Heat Transfer 2, Computational Mechanics Publication, Southampton, Boston, 1990.
[13] T.H. Kuehn, R.J. Goldstein, An experimental study and theoretical study of natural convection in the annulus between horizontal concentric cylinders, J. Fluid Mech. 74 (1976) 695–719.
[14] U. Projahn, H. Rieger, H. Beer, Numerical analysis of laminar natural convection between concentric and eccentric cylinders, Numer. Heat Transfer 4 (1981) 131–146.
[15] K. Sasaguchi, K. Kuwabara, K. Kusano, H. Kitagawa, Transient cooling of water around a cylinder in a rectangular cavity – a numerical analysis of the effect of the position of the cylinder, Int. J. Heat Mass Transfer 41 (1998) 3149–3156.
[16] J.F. Thompson, Z.U.A. Warsi, C.W. Mastin, Numerical Grid Generation, North-Holland (1985) 188–235.
[17] H.A. van der Vorst, BICGSTAB: A fast and smoothly convergence variant of BI-CG for the solution of non symmetric linear systems, SIAM J. Sci. Stat. Comput. 13 (1992) 631–644.
[18] M.N. Özisik, Finite Difference Methods in Heat Transfer, CRC Press, London, 1994.
[19] Q.H. Deng, G.F. Tang, Numerical visualization of mass and heat transport for conjugate natural convection/heat conduction by streamline and heatline, Int. J. Heat Mass Transfer 45 (5) (2002) 2373–2385.
[20] I. Demirdžić, Ž. Lilek, M. Perić, Fluid flow and heat transfer test problems for non-orthogonal grids: bench-mark solutions, Int. J. Numer. Methods Fluids 15 (1992) 329–354.